JOURNAL OF MATERIALS SCIENCE 25 (1990) 2667–2678

Estimates of internal stresses about interstitials in a bcc lattice

BAOPING HE, SATISH RAO, C. R. HOUSKA
Department of Materials Engineering, Virginia Polytechnic Institute and State University, Blacksburg, Virginia 24061, USA

The atomic volume of interstitial cubic and hexagonal interstitial compounds has been found to correlate with the size of the filled octahedron in corresponding dilute solutions. Data from binary systems containing N, C, and O in V, Nb, Ta, Cr, Mo, W, and Fe lattices were examined. Systematic correlations enable estimates to be made of the components of the dipole tensor for interstitials in octahedral sites within selected bcc lattices. The volume change in filling an interstitial site is used to determine the sum of the diagonal tensor components, while their ratio is obtained from the second-neighbour displacement of a lattice atom about a filled site. Estimates from crystallographic data are obtained using either a volume correlation or a common shape factor along with the second-neighbour displacement. A filled octahedron tends to give equal first and second-neighbour distance parameters making it nearly regular. Estimates are made from isotropic and anisotropic elasticity. Lattice Green function calculations support the use of the second neighbour as a core displacement parameter. As expected, core displacements obtained from lattice theory can differ greatly from those obtained by elastic calculations except for the second-neighbour displacement. The influence of crystal anisotropy on the long range elastic field is examined. In niobium the first neighbour is displaced along an elastically soft direction and one finds the largest displacements of any system examined.

1. Introduction

When an interstitial atom, such as carbon, nitrogen or oxygen atom is introduced into a metal crystal, displacements occur in the lattice surrounding the interstitial atom. This is especially large in bcc metals, like group VA, VIA and VIIIA transition metals (V, Nb, Ta, Cr, Mo, W and Fe). The long range displacement field is determined from the stress dipole tensor and the elastic constants of the pure host metals. A knowledge of the stress dipole tensor for an interstitial alloy system is required for fundamental interpretations of physical properties [1]. X-ray intensity data, obtained from ion-implanted bcc metals, such as molybdenum and niobium films implanted with nitrogen at liquid nitrogen temperature, can be greatly influenced by static atomic displacements about these point-like defects [2, 3]. Because of its fundamental importance and the difficulties encountered for making direct measurements with many bcc metals, we have examined ways of making estimates of this tensor using known crystallographic data and parametric approaches.

Many works have been published on the measurement of the stress dipole tensor using internal friction [4], ultrasonic waves [5], X-ray scattering [6, 7], lattice swelling measurements [8, 9], and other techniques [10, 11]. The measured values have been summarized by Tewary [4] and Shirley [12], but unfortunately these data are available for only a few systems.

It has been suggested that the first and second-neighbour displacements can be estimated from corresponding compound information [2, 3]. This has been examined more completely by using all of the available crystallographic data, for the previously mentioned metals and interstitials. The stress dipole tensor is estimated for carbon, nitrogen or oxygen interstitials located at octahedral sites in bcc crystals of V, Nb, Ta, Cr, Mo, W and Fe and compared with the available data.

2. Crystallography of interstitial sites

The octahedral interstitial sites in bcc, fcc and hcp structures are shown in Fig. 1. This site in a bcc lattice is irregular, with a distance between the central point and the two first-neighbour atoms of $a/2$, and $a/\sqrt{2}$ for the four second-neighbour atoms (see Fig. 1a). Octahedral sites in fcc structures are regular, with a distance between an interstitial and its six first-neighbour atoms of $a/2$ (see Fig. 1b). Likewise octahedral sites in an ideal hcp structure (with $c/a = \sqrt{8/3}$) are regular and surrounded by six atoms at a distance of $(a^2/3 + c^2/16)^{0.5} = a/\sqrt{2}$ (see Fig. 1c). For a non-ideal hcp lattice with $c/a \neq \sqrt{(8/3)}$, six edges of length a are located in (0001) planes and six extend diagonally between them with lengths $b = (a^2/3 + c^2/4)^{0.5}$. These adjustments in the non-ideal hcp lattice do not alter the first-neighbour coordination number which remains at six metal atoms separated

0022–2461/90 $03.00 + .12 © *1990 Chapman and Hall Ltd.*

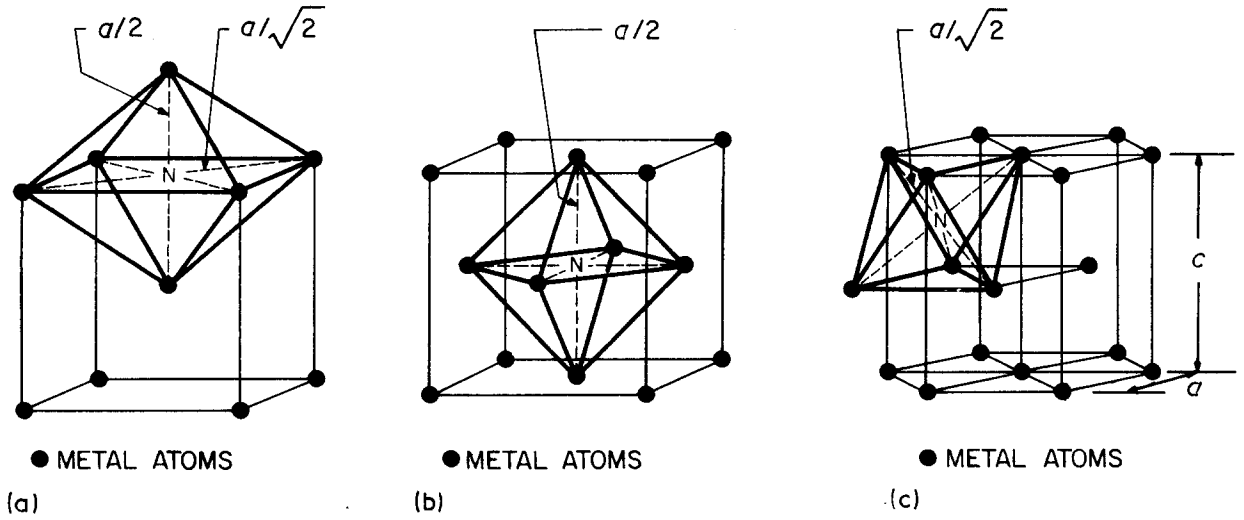

Figure 1 (a) Irregular octahedral site in a bcc lattice, (b) regular octahedral site in a fcc lattice, and (c) an octahedron in a hcp lattice (● metal atoms).

by $(a^2/3 + c^2/16)^{0.5}$. The distortion of the non-ideal octahedron can be seen from an examination of the angular distortion between two diagonals, $\Delta\beta$, i.e.

$$\Delta\beta = 2\tan^{-1}[1/3 + (c/2a)^2]^{0.5} - 90° \quad (1)$$

At $c/a = (8/3)^{0.5}$, $\beta = 90°$. For the structures considered, c/a varies from 1.58 to 1.65, causing $\Delta\beta$ to vary over the range of $-1.25°$ to 0.40°. Therefore, the octahedra in hcp lattices that we will consider are regular within a small angular distortion. One can see these distortions by viewing a regular octahectron along the tetragonal axis (z), fixing a, and allowing c to vary above and below the ideal value. This is illustrated in Fig. 2.

When all known compounds of V, Nb, Ta, Cr, Mo, W, Fe with C, N and O are examined, an irregular octahedral site in a bcc lattice attempts to become a regular octahedron within its compound. There are usually several compounds for a given system and each gives a somewhat different octahedron size. For example, in the Nb–N system, Nb_2N with hcp structure ($a = 0.3056$ nm, $c = 0.4995$ nm) gives first-neighbour Nb–N distance of 0.2162 nm, while NbN with the NaCl structure ($a = 0.4394$ nm) gives a Nb–N distance of 0.2197 nm. It can be reasoned [13] that for either a hcp or fcc metal lattice one octahedral site corresponds to one metal atom, so that those compounds with chemical formula MI have all interstitial sites filled. The octahedron volume calculated from a partially filled compound (M_2I) is always smaller than for one that is filled (MI) and structure data do not show a size difference for filled and unfilled octahedra in M_2I type compounds. If one exists, it must be small enough to escape detection in a routine structure analysis. It will be shown later that the octahedron volume in the filled compound differs from that of a filled site in the dilute solution.

The first-neighbour and second-neighbour displacements, required to reshape the irregular octahedron in the pure bcc metal into a regular octahedron in a NaCl type MI compound are given by the following equations

$$d_1 = 0.5(a_{MI} - a_{bcc}) \quad (2a)$$

$$d_2 = 0.5(a_{MI} - \sqrt{2a_{bcc}}) \quad (2b)$$

For a hcp type MI compound, we obtain

$$d_1 = (a^2/3 + c^2/16)^{0.5} - a_{bcc}/2 \quad (3a)$$

$$d_2 = (a^2/3 + c^2/16)^{0.5} - a_{bcc}/\sqrt{2} \quad (3b)$$

Further investigation shows that a one-to-one relation between octahedra and host atoms is also true for the bcc structure. In dilute bcc lattice, the c axis of the tetragonal distortion is directed along (1 0 0), (0 1 0) and (0 0 1) so that the space can be filled by irregular octahedra as shown. For a filled bct lattice aligned in the same direction there is one interstitial site corresponding to one host atom.

It is well known from the Bain correspondence [14] that a fcc lattice may be alternatively described as a bct lattice with $c/a = \sqrt{2}$. It follows that a fictitious bct lattice can be made to extend from the pure bcc dilute solution, to a partially filled compound, and finally to a filled NaCl type compound. In this sequence, the c/a ratio varies from 1 to $\sqrt{2}$ as the fraction of octahedral sites, x, varies from 0 to 1 and all interstitials are aligned in one direction. There is a gap between this model and a dilute cubic solution where the interaction between interstitials is negligible so that their fields remain randomly oriented along all three directions. A random configuration is likely for a system implanted at a low enough temperature so

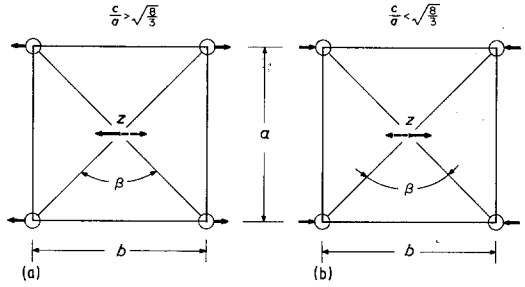

Figure 2 Two distorted octahedra in the hcp lattice of Fig. 1c viewed along the normal to the plane of four nearest neighbours. Note that in (a) $b > a, \beta > 90°$ and in (b) $b < a, \beta < 90°$. In each case, c is not perpendicular to the plane containing a and b. The solid central vector extends out of the plane toward the viewer.

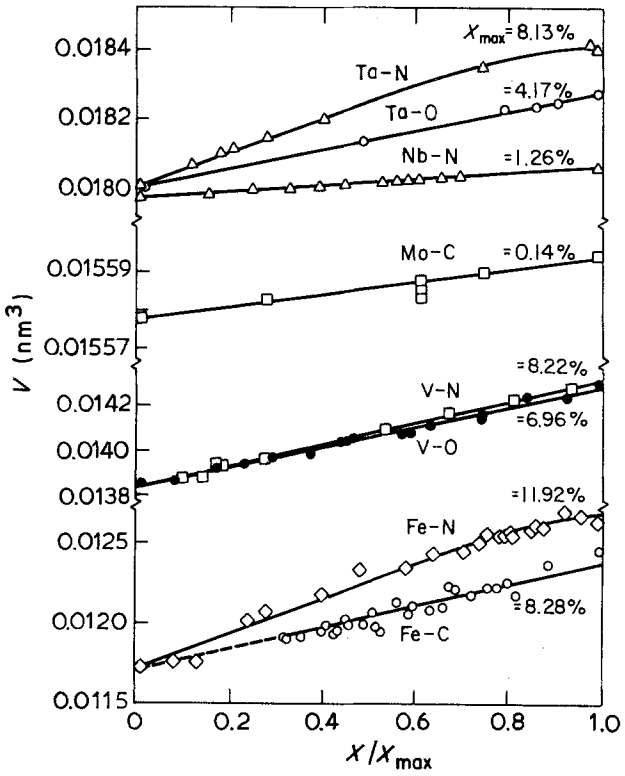

Figure 3 Atomic volume plotted against fraction of occupied octahedra in dilute solutions, for Ta–N [19], Ta–O [20], Nb–N [19], Mo–C [21], V–N [22], V–O [23], Fe–N [24] and Fe–C [24]. Values of X_{max} are given at the extreme right.

that all transport mechanisms for foreign interstitials become inoperative.

The b c t lattice parameters c and a and unit cell volume are given by [15]:

$$c = a_0(1 + u_{33}x) \quad (4a)$$

$$a = a_0(1 + u_{11}x) \quad (4b)$$

$$V = a_0^3[1 + (2u_{11} + u_{33})x] \quad (4c)$$

Here x is the fraction of the occupied octahedral sites, a_0 the lattice parameter of the b c c host lattice and u_{11} and u_{33} components of the distortion tensor. Terms beyond the first two in Equation 4c are dropped for a dilute solution making it linear. Equations 4a to c represent a fictitious model when extended from the pure b c c lattice to full occupation of octahedral sites. It is fictitious in that it does not allow for lattice relaxations that accompany compound formation.

3. Atomic volume change in a dilute solution

We define the atomic volume of an interstitial alloy by

$$V = \frac{\text{Volume of unit cell}}{\text{Number of metal atoms in unit cell}} \quad (5)$$

Atomic volume clearly includes the volume of each metal atom plus a contribution from the interstitials. This definition will be used later for all types of structures in interstitial alloys.

For the interstitial alloys under consideration, bonding is taken to be metallic making the atomic volume nearly independent of the crystal structure for a given composition. This is shown in Table I which provides a listing of atomic volume for interstitial systems having different crystal structures with the same chemical formula. These results suggest that pseudo compounds with either a h c p or f c c structure can be established which is based upon the atomic volume of a compound having a structure that is neither hexagonal nor f c c. This behaviour is well known for metallic substitutional solutions and for our purposes conveniently defined in [18]. It has been stated that "Provided the nature of the interatomic forces remains essentially metallic, the atomic volume so defined is independent of the crystal structure of the material". With sufficiently dilute solutions the atomic volumes of solid solutions vary linearly with the atomic concentration of the solute.

By analogy, we can consider a binary interstitial alloy system as a system comprised unoccupied and occupied octahedra within a metal lattice. The occupied octahedra are substituted for unoccupied octahedra with increasing interstitial content. The atomic volume of eight dilute solutions are plotted against the interstitial content and are found to be nearly linear (Fig. 3). When this is extended over the full range for compounds of Nb–N, one finds a considerable departure from Vegards law (Fig. 4).

For an interstitial alloy, we have taken Vegards law to mean a linear relation between atomic volume and the fraction of occupied octahedra. This is true only for the dilute solution. Here atomic volume is used instead of octahedron volume. However, these

TABLE I Atomic volume of interstitial compounds [16, 17]

Chemical formula	Crystal structure	Atomic volume
MoC	WC	20.43
	AsTi	20.42
Mo_2C	NaCl	19.25
	O_2Pb	18.15
	Mo_2C	18.58
	hp*	18.73
Nb_2C	hp*	20.86
	Nb_2C	20.98
V_2C	Fe_2N	22.30
	O_2Pb	22.06
WC	WC	20.75
	NaCl	20.38
W_2C	O_2Pb	18.20
	Fe_2N	18.20
	I_2Cd	18.43
CrN	NaCl	17.84
	CrN	17.67
Fe_2N	O**	14.68
	Ni_3Ti	14.61
	hcp	14.62
NbN	AsNi	21.11
	NaCl	21.21
	AsTi	21.36
	WC	21.06
Ta_2N	V_2N	19.83
	Fe_2N	19.78
WN	t**	20.64
	WC	20.48

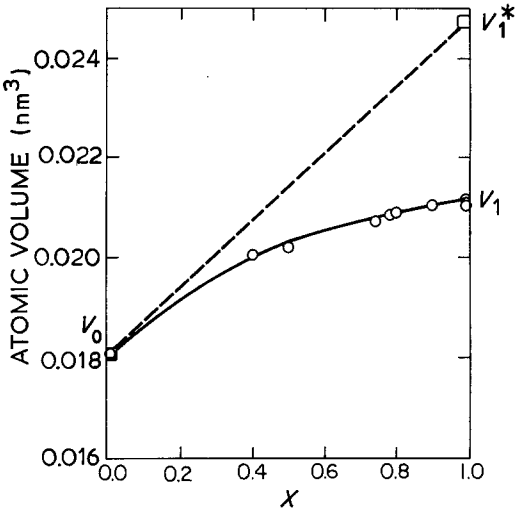

Figure 4 Atomic volume plotted against fraction of occupied octahedra compared with an extrapolation of dilute solution data for the Nb–N system.

quantities are linearly related since the average octahedron volume calculated from the lattice parameters is 2/3 of the atomic volume for bcc, fcc and hcp structures. The atomic volume corresponding to occupied octahedra in a dilute solution is referred to as an effective atomic volume, V_1^*, which can be evaluated by extrapolating the linear relation of a dilute solution to $x = 1$. Atomic volume given by Vegards law for a dilute interstitial system (or the fictitious one extending the $x = 1$) is

$$V_x^* = V_0(1 - x) + xV_1^* \quad (6)$$

where, V_0 is atomic volume of the metal atom in the bcc lattice of the pure element. The ratio of V_x^* to V_x as seen in Fig. 4 represents the deviation from Vegards law for each compound MI_x.

$$R_x = V_x^*/V_x \quad (7)$$

V_x is atomic volume calculated from the real compound using Equation 5. At $x = 1$, we obtain R_1, with V_1 representing the atomic volume calculated from MI type compounds with all octahedral sites occupied. Table II provides R_1 for several systems obtained from measured $1/V\,\delta V/\delta C$ values and lattice parameters of MI compounds.

Since there are no MI type compounds for Fe–N and Fe–C systems, V_1 are obtained from other related compounds. Atomic volumes for M_2I and MI type compounds are calculated from

$$V_{0.5} = \frac{\sqrt{3}a^2c}{4}\ (\text{hex}) \quad (8a)$$

and

$$V_1 = \frac{a^3}{4}\ (\text{NaCl}) \quad (8b)$$

The ratio of $V_{0.5}$ to V_1 for Nb–C, V–C, Ta–C, Mo–C and W–C is nearly a constant as is seen in Table III. If we take the average ratio of $\langle V_{0.5}/V_1\rangle = 0.923$ to approximate this ratio for the Fe–C system, we can estimate the atomic volume of a psuedo NaCl type compound. For FeC, one finds

$$V_1(\text{Fe–C}) = \frac{V_{0.5}(\text{Fe–C})}{0.923} = 0.01546\,\text{nm}^3 \quad (9)$$

as well as the lattice parameter, $a = 0.3954$ nm. Similar reasoning is used for estimating the atomic volume for other non-existent MI type compounds which are indicated by a parenthesis in Table IV. The second-neighbour displacements listed in Table V were calculated from the data in Table IV and Equations (2b and 8b).

From the V_1^*/V_1 ratio in Table II, an average value of

$$\langle R_1\rangle = 1.20 \quad (10)$$

is obtained with maximum variation of less than 7%. This empirical constant is used later to estimate stress dipole tensors for systems without supporting lattice parameter data for dilute solutions.

The fractional change in volume with x may be obtained by differentiating Equation 6. This can also be equated to the atomic fraction of the interstitial element C, for a dilute solution i.e.

$$\frac{1}{V}\frac{\partial V}{\partial x} = \frac{1}{V}\frac{\partial V}{\partial C}$$

since

$$C = x/(1 + x) \approx x$$

therefore

$$\frac{1}{V}\frac{\partial V}{\partial C} = \frac{V_1^* - V_0}{V_0} \quad (11)$$

and by using Equation 10, $V_1^* \approx 1.2\,V_1$. The latter is an interesting result because it allows the fractional volume change due to the addition of interstitials to be estimated from known atomic volumes. Experimentally, the interstitial solubilities may be so low that the results are unreliable. First- and second-neighbour displacements have been calculated from the octahedron size in NaCl type compounds using Equations 2a and b.

When the shape of the octahedron is known for the dilute solution, the volume is obtained from the second-neighbour displacement. First- and second-neighbour distances are defined by

$$r_1 = \frac{a}{2}(1 + \varepsilon_{33}),\ r_2 = \frac{a}{\sqrt{2}}(1 + \varepsilon_{11}) \quad (12)$$

with $a/\sqrt{2}$, and $a/2$ for bcc. Their ratio defines the shape factor

$$S = \frac{1 + \varepsilon_{33}}{1 + \varepsilon_{11}} \quad (13)$$

TABLE II Values of R_1 and S

	V–N	Nb–N	Ta–N	Fe–N	V–O	Ta–O	Mo–C	Fe–C
R_1	1.155	1.166	1.163	1.280	1.180	1.144	1.282	1.277
S	1.453	1.494	1.453	1.515	1.479	1.431	–	1.560

TABLE III Atomic volume (nm^3) estimation

Chemical formula and crystal structure			Nb–C	V–C	W–C	Ta–C	Mo–C	Fe–C
Me_2I	hcp	$V_{0.5}$	0.02105	0.01669	0.01830	0.02066	0.01846	0.01427
MeI	NaCl	V_1	0.02233	0.01800	0.02038	0.02190	0.02043	(0.01546)
		$V_{0.5}/V_1$	0.943	0.927	0.898	0.943	0.904	⟨0.923⟩

TABLE IV Atomic volume (nm^3) of MeI type structure of 17 interstitial alloy systems

	V	Nb	Ta	Cr	Mo	W	Fe
MeC	0.01800	0.02233	0.02190	(0.01821)	0.02043	0.02038	(0.01546)
MeN	0.01769	0.02121	0.02268	0.01784	0.01989	0.02048	(0.01583)
MeO	0.01722		0.02187	0.01800			

which is equal to $\sqrt{2}$ for a regular octahedron. Taking

$$2\varepsilon_{11} + \varepsilon_{33} = \frac{V_1^* - V_0}{YV_0} \tag{14}$$

and since ε_{11} and ε_{33} refer to an infinite medium, the Eshelby factor, Y, is introduced. This is defined later. Equations 13 and 14 combine to give

$$\frac{V_1^* - V_0}{YV_0} = S - 1 + (2 + S)\varepsilon_{11} \tag{15}$$

S has been found to vary by less than 6% about an average value of 1.48. This allows the volume change to be calculated from the second-neighbour displacement.

4. Dipole stress tensor and elastic displacement fields

The experimental change in fractional volume and the second-neighbour displacement can be used to estimate the dipole stress tensor. The simplest calculation makes use of an isotropic elasticity calculation; however, it is also the most approximate except for tungsten. A second approach using the same input parameters makes use of the elastic Green function and has the advantage of treating elastic anisotropy. For isotropic tungsten, both approaches are in agreement as expected.

The elastic displacement field about an interstitial atom is an octahedral interstitial site within an infinite isotropic crystal has been given by Keating and Goland [28], i.e.

$$u^{\alpha} = i_r\left(\frac{D}{r^2} + \frac{E\cos^2\theta}{r^2}\right) + i_\theta \frac{F}{r^2}\sin\theta\cos\theta \tag{16}$$

where

$$D = -\left(\frac{\lambda + \mu}{2\mu}\right)C_d + C_s; \quad E = \frac{5\mu + 3\lambda}{2\mu}C_d$$

$$F = -C_d$$

$$\lambda = \tfrac{1}{5}(C_{11} + 4C_{12} - 2C_{44})$$

$$\mu = \tfrac{1}{5}(C_{11} - C_{12} + 3C_{44})$$

where C_s and C_d are the strengths of the spherical and doublet displacement fields, i_r and i_θ are unit vectors in a spherical polar coordinate system centred on the doublet force, r is the distance from the centre and θ is the angle between r and the axis of the doublet force aligned along any one of the equivalent directions. λ and μ are the Lame elastic constants. The bulk strain produced by a uniform distribution of interstitials in the z type of octahedral site, with the axis of the doublet force along the [001] direction, is given by

$$u_{11} = \frac{4\pi}{3}\left(\frac{x}{V_0}\right)Y\left(C_s - \frac{\lambda}{2\mu}C_d\right) \tag{17a}$$

$$u_{33} = \frac{4\pi}{3}\left(\frac{x}{V_0}\right)Y\left(C_s + \frac{\lambda + \mu}{\mu}C_d\right) \tag{17b}$$

TABLE Va The first-neighbour displacement, d_1 (nm) and per cent strain (%) relative to original distance for 17 interstitial alloy systems. Obtained from structure data

		V	Nb	Ta	Cr	Mo	W	Fe
C	d	0.057	0.058	0.058	(0.065)	0.060	0.059	(0.054)
	%	37.4	35.2	34.9	45.1	37.9	37.0	37.9
N	d	0.055	0.054	0.060	0.063	0.058	0.059	(0.056)
	%	36.6	32.9	36.5	44.1	36.7	37.2	39.1
O	d	0.054		0.057	0.064			
	%	35.4		34.9	44.5			

TABLE Vb The second-neighbour displacement, d_2 (nm) and per cent strain (%) relative to original distance for 17 interstitial alloy systems. Obtained from structure data

		V	Nb	Ta	Cr	Mo	W	Fe
C	d	−0.006	−0.010	−0.011	(+0.005)	−0.006	−0.007	(−0.009)
	%	−2.8	−4.3	−4.7	2.5	−2.7	−3.1	−4.4
N	d	−0.007	−0.014	−0.008	+0.004	−0.007	−0.007	(−0.005)
	%	−3.3	−6.0	−3.4	2.0	−3.1	−3.1	−2.5
O	d	−0.009		−0.011	+0.004			
	%	−4.2		−4.7	2.0			

where x is the fraction of z type sites occupied and $Y = 3(\lambda + 2\mu)/(3\lambda + 2\mu)$ factor first introduced by Eshelby [29] to meet the boundary conditions on the free surface of the crystal. If the crystal has cubic symmetry, all three types of equivalent sites are filled with equal probability and

$$\frac{1}{V}\frac{\partial V}{\partial C} = \frac{4\pi}{3V_0} Y(3C_s + C_d) \quad (18)$$

where C is the atomic fraction of the impurity atoms. Similarly from Equation 18 the sum of components of the elastic dipole stress tensor for an octahedral defect oriented along the z direction becomes [30]

$$2P_{11} + P_{33} = (3\lambda + 2\mu)\frac{\partial V}{\partial C} \quad (19)$$

One can show that the sum of the components of the dipole stress tensor is give by

$$2P_{11} + P_{33} = (3\lambda + 2\mu)\frac{4\pi Y}{3}(3C_s + C_d) \quad (20)$$

The fractional change in volume with atomic fraction, as given in Equations 18 and 19, provide a link with lattice parameter data as was shown in the previous discussions. However, a second experimental parameter is required in order to evaluate the strength parameters and both components of the dipole tensor. Table V shows that the first-neighbour displacement from compound data is normally large while the second-neighbour displacement is small for a core displacement and is typically less than 5% of the second-neighbour distance. This has been selected as the second experimental parameter to be fitted to the linear elastic equations. Proceeding on this basis using Equation 16, we obtain

$$d_2 = \frac{1}{a^2}\left(2C_s - \frac{\lambda + \mu}{\mu}C_d\right) \quad (21)$$

From Equations 16 and 18, one can solve for the separate strengths in terms of the volume change and the second-neighbour displacement i.e.

$$C_s = \left(\frac{\lambda + \mu}{3\lambda + 5\mu}\right)\frac{3V}{4\pi Y}\left(\frac{1}{V}\frac{\partial V}{\partial C}\right) + \left(\frac{\mu}{3\lambda + 5\mu}\right)d_2a^2 \quad (22a)$$

$$C_d = \left(\frac{2\mu}{3\lambda + 5\mu}\right)\frac{3V}{4\pi Y}\left(\frac{1}{V}\frac{\partial V}{\partial C}\right) - \left(\frac{3\mu}{3\lambda + 5\mu}\right)d_2a^2 \quad (22b)$$

or, in terms of the dipole stress tensor

$$C_d = \frac{P_{33} - P_{11}}{4\pi(\lambda + 2\mu)} \quad (23a)$$

$$C_s = \frac{P_{11}}{4\pi(\lambda + 2\mu)} \quad (23b)$$

Solving for the components of the dipole stress tensor, gives the simplest estimate based upon isotropic elasticity theory

$$P_{11} = P_{22} = 4\pi\left(\frac{\lambda + 2\mu}{3\lambda + 5\mu}\right)\left((\lambda + \mu)\frac{3V}{4\pi Y}\frac{1}{V}\frac{\partial V}{\partial C} + \mu d_2a^2\right) \quad (24a)$$

$$P_{33} = 4\pi\left(\frac{\lambda + 2\mu}{3\lambda + 5\mu}\right)\left((\lambda + 3\mu)\frac{3V}{4\pi Y}\frac{1}{V}\frac{\partial V}{\partial C} - 2\mu d_2a^2\right) \quad (24b)$$

The dipole stress tensor can also be estimated from the displacement field around an interstitial by an anisotropic elasticity theory. Beyond the core region, the displacements are given by [29]

$$u_i(\boldsymbol{r}) = G^{el}_{ij,k}(\boldsymbol{r})P_{jk} \quad (25a)$$

where $u_i(\boldsymbol{r})$ $(i = 1, 2, 3)$ are the cartesian component of displacement at vector position $\boldsymbol{r}$ with respect to the interstitial, $G^{el}_{ij,k}$ is the elastic Green function of the ideal lattice with a derivative taken in the k direction. The dipole stress tensor is estimated by making the volume change and the second-neighbour displacement agree with the crystallographic values. This fitting procedure was carried out at 10 nm along the [110] direction using Equation 21 which is assumed to be an elastic displacement. The isotropic displacement serves as a starting estimate for the anisotropic approach i.e. Equation 25a. These components P_{11}, P_{33} along with some experimentally measured values are listed in Tables VI, VII and VIII for V, Nb, Ta, Cr, Mo, W and Fe with solutes C, N and O.

5. Calculated displacement fields

The long range atomic displacement field is calculated from Equation 25a. For the core displacements this elastic approach is modified to include anharmonicity in the host lattice. This modification is given by

$$u_i^m = \sum_{j,n} G_{ij}^{m-n} f_j^n \quad (25b)$$

TABLE VI Components P11, P22 and P33 of stress tensor in (eV) for systems containing V–N, Nb–N, Ta–N, Fe–N, V–O, Nb–O and Ta–O. Estimates are based upon experimental volume changes and crystallographic second neighbour distances

Method	Elastic theory		V–N	Nb–N	Ta–N	Fe–N	Fe–C	V–O	Ta–O
Crystal structure data	Isotropic Theory	P_{11}	4.53	4.64	6.68	6.04	4.76	4.15	4.74
		P_{33}	10.14	12.31	17.25	15.44	16.33	10.43	16.35
	Anisotropic Theory	P_{11}	4.28	3.70	7.37	6.98	6.07	3.86	5.56
		P_{33}	10.64	14.19	15.86	13.56	13.71	11.00	14.71
Measured values		(P_{11})	4.13	4.39	7.10	7.03	6.37	3.82	6.58
		P_{33}	10.94	12.81	16.40	13.46	13.11	11.08	12.66
		$2P_{11} + P_{33}$	19.20	21.59	30.60	27.52	25.85	18.72	25.82
Reference			[12]	[25]	[12]	[26]	[27]	[7]	[25]

TABLE VII Estimated stress tensor in (eV) for systems containing V–N, Nb–N, Ta–N, Fe–N, V–O, and Ta–O. Estimates are based upon crystallographic second-neighbour distances and shape factor $\langle S \rangle = 1.484$ or atomic volume ratio $\langle R_1 \rangle = 1.2$

Method	Elastic theory		V–N	Nb–N	Ta–N	Fe–N	Fe–C	V–O	Ta–O
Average atomic volume ratio $\langle R_1 \rangle = 1.20$	Isotropic	P_{11}	5.12	5.38	7.50	5.32	4.60	4.43	5.97
	Theory	P_{33}	11.11	13.30	18.72	12.75	12.72	10.85	18.31
	Anisotropic	P_{11}	4.81	4.42	8.22	6.04	5.45	4.08	6.80
	Theory	P_{33}	11.73	15.23	17.30	11.32	11.03	11.55	16.65
		$2P_{11} + P_{33}$	21.35	24.07	33.74	23.40	21.93	19.71	30.25
Average shape factor $\langle S \rangle = 1.48$	Isotropic	P_{11}	4.95	4.48	7.74	6.35	5.55	4.24	6.11
	theory	P_{33}	10.84	12.02	19.11	14.67	14.49	10.55	18.53
	Anisotropic	P_{11}	4.65	3.56	8.47	7.12	6.45	3.90	6.95
	theory	P_{33}	11.44	13.85	17.66	13.12	12.69	11.23	16.85
		$2P_{11} + P_{33}$	20.74	20.97	34.60	27.36	25.59	19.03	30.75

where u_i^m ($i = 1, 2, 3$) are the cartesian components of displacements of the m^{th} lattice atom, $G_{ij}^{m-n}s$ the Green function matrix of the ideal lattice and f_j^n are the cartesian components of the Kanzaki forces acting on the n^{th} lattice atom. The Kanzaki forces are not only due to the defect–lattice interaction but they also model any anharmonicity in the host lattice displacement field. For points far away from the defect, Equation 25b must converge to the harmonic elastic solution Equation 25a.

The Kanzaki forces are related to the dipole stress tensor by

$$\sum_n r_i^n f_j^n = P_{ij} \tag{25c}$$

where r_i^n are the cartesian components of the vector joining the interstitial site with the n^{th} lattice atom. If radial Kanzaki forces are assumed to act only on the first three neighbouring shells around the interstitial defect, then

$$P_{11} = f^{(1)}a + \frac{4f^{(3)}a}{\sqrt{5}}$$

and

$$P_{22} = \sqrt{2}f^{(2)}a + \frac{8f^{(3)}a}{\sqrt{5}}$$

It has been shown that for b c c niobium and tantalum, forces must be applied to the first three neighbours in order to be in reasonable agreement with the data [31]. All three are evaluated by using the two components of the stress tensor and the second-neighbour distance given by the compound. Core displacements are calculated using the lattice Green function and the Kanzaki forces given in Table IX. The elastic displacement field far away from the defect remains the same for both the models, since they are determined by the same dipole tensor and the elastic constants of the b c c crystal (Equation 2).

Tables Xa and Xb give displacement fields using anisotropic Green function calculations (Equations 25a and 25b). These may be compared with the isotropic calculations of Keating and Goland as given in Equation 25c. We have carried out both calculations for eight systems using common dipole tensors and second-neighbour distances.

An examination of atomic displacements about interstitials in a dilute solution, using the lattice Green function, indicates that major positive displacements are found along the tetragonal axis and minor negative displacements occur in perpendicular directions. Also, no sharp transition is found between lattice or atomistic calculations and those based upon a purely elastic calculation.

The literature shows that when different calculations are compared [28] large differences in the core displacements are found. These differences between various calculations are at a minimum at the second and more distant neighbours along equivalent [110] directions. An examination of Table X shows that lattice calculations give a smaller first-neighbour displacement than elastic calculations. The latter are extrapolations of a linear theory into a region of large displacements where departures are expected. With the exception of the first-neighbour displacement, all strains should be small enough to be in accord with a linear theory. Oscillations in the lattice displacements account for the major departures with those obtained

TABLE VIII Estimated stress tensor in (eV) for systems containing V–C, Nb–C, Ta–C, Cr–C, Cr–N, Cr–O, Mo–C, Mo–N, W–C and W–N. Estimates are based upon crystallographic second-neighbour distances and shape factor $\langle S \rangle = 1.484$ or atomic volume ratio $\langle R_1 \rangle = 1.2$. No experimental dipole tensor

Method	Elastic theory		V–C	Nb–C	Ta–C	Cr–C	Cr–N	Cr–O	Mo–C	Mo–N	W–C	W–N
Average atomic volume ratio $\langle R_1 \rangle = 1.20$	Isotropic	P_{11}	5.56	7.11	6.02	8.22	7.51	7.81	9.84	8.28	9.64	9.99
	Theory	P_{33}	11.30	14.23	18.34	11.85	12.03	11.97	25.21	25.04	30.79	30.82
	Anisotropic	P_{11}	5.32	6.32	6.87	8.20	7.37	7.75	8.75	7.05	9.64	9.99
	Theory	P_{33}	11.78	15.82	16.64	11.89	12.31	12.17	27.39	27.50	30.79	30.82
		$2P_{11} + P_{33}$	22.42	28.46	30.38	28.29	27.05	27.59	44.89	41.60	50.08	50.80
Average shape factor $\langle S \rangle = 1.48$	Isotropic	P_{11}	5.41	6.19	6.17	10.83	10.04	10.38	11.27	9.56	11.81	12.19
	theory	P_{33}	11.03	12.92	18.56	17.60	17.54	17.57	27.80	27.36	34.78	34.87
	Anisotropic	P_{11}	5.17	5.35	6.98	10.61	9.71	10.09	10.14	8.26	11.81	12.19
	theory	P_{33}	11.51	14.60	16.93	18.05	18.21	18.15	30.06	29.96	34.78	34.87
		$2P_{11} + P_{33}$	21.85	25.30	30.89	39.27	37.63	38.33	50.34	46.48	58.40	59.24

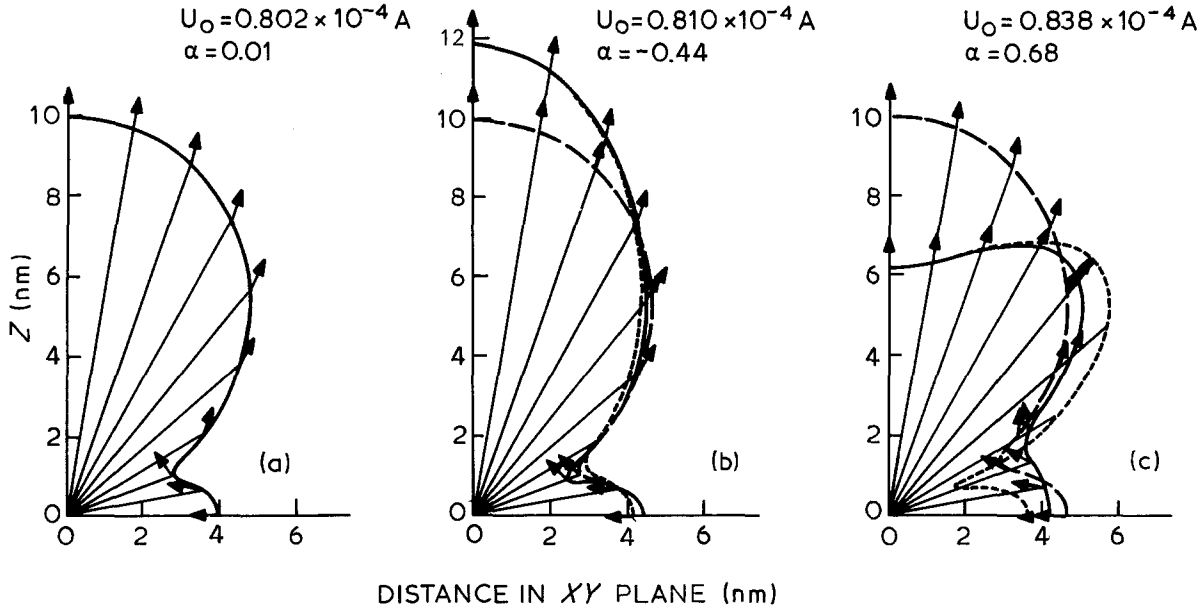

Figure 5 Locus of elastic displacements of constant magnitude for three systems (a) W–N, ($u_0 = 0.802 \times 10^{-5}$ nm, $x = 0.01$), (b) Mo–N ($u_0 = 0.810 \times 10^{-5}$ nm, $\alpha = -0.44$) and (c) Ta–N ($u_0 = 0.838 \times 10^{-5}$ nm, $x = 0.68$) with very different lattice anisotropy showing isotropic (— —) and anisotropic solutions (——, - - -). Vector directions in (100) (——) and (110) (- - -) planes along the same radial angle are essentially the same.

from purely elastic calculations. The calculations given in Table X represent fields from single interstitial defects while the dilute solution data presented in Fig. 3 extend to ~8 at %. Clearly there is considerable overlap of displacement fields in regions extending beyond the first and second neighbours. Averaging these interacting fields should tend to smooth out the oscillations.

The octahedron model introduces correlation between first and second neighbours that leads to the correct change in volume when expressed in terms of the second-neighbour displacement. The latter is small and most consistent with respect to lattice and elastic calculations. The first-neighbour displacements calculated from the octahedron model need not agree with the actual lattice values but rather are parameters that give the components of the dipole stress tensor within ~20% of the experimental values. One finds that these first-neighbour parameters tend to be intermediate relative to those obtained from both lattice and anisotropic elastic calculations.

In applying anisotropic approaches, the following parameter plays an important role

$$\alpha = C_{44} - 0.5(C_{11} - C_{12}) \qquad (26)$$

These are listed for seven host metals in Table XI. They provide useful data for discussing the elastic displacement fields in anisotropic lattices. Figs 5a, b and c show polar plots of the locus of displacements of constant magnitude around an interstitial defect. An intermediate and two extreme systems are illustrated in terms of their elastic anisotropy, α. The tetragonal axis is denoted by C and the direction of the displacements are indicated at 10° intervals. Fig. 5b shows a plot at radial distances for the Mo–N system, with a constant displacement of $u_0 = 0.81 \times 10^{-5}$ nm. The anisotropic solution gives an equidisplacement point farther from the defect than does the isotropic solution along the C axis when α is negative. Fig. 5c shows a similar plot for the Fe–C system in which the anisotropic solution gives an equi-displacement point along C axis closer to the defect because of the positive α. Fig. 5a is an intermediate plot for the W–N system. In this case, the three curves are essentially identical because tungsten may be considered to be isotropic ($\alpha = 0.01$).

Fig. 6 is the polar plot of the Nb–N system in which the anisotropic solution gives significantly larger displacements relative to any of the systems examined. This becomes obvious from the large value of u_0 at larger distances along C and in perpendicular directions (Fig. 6). In niobium, the [0 0 1] direction is elastically soft, causing large positive displacements while the perpendicular direction responds with a large Poisson contraction.

6. Discussion

An examination of crystallographic data has shown that the atomic volume of interstitial compounds combining N, C, and O with V, Nb, Ta, Cr, Mo and W having different crystal structures with the same chemical formula is nearly a constant. One also finds that the ratio of atomic volume of hcp (M_2I) compounds to cubic NaCl type structures (MI) is ~0.923.

TABLE IX Kanzaki forces, $f^{(1)}$, $f^{(2)}$ and $f^{(3)}$, in (eV A^{-1}) acting on the first three neighbouring shells around an interstitial atom

	V–N	Nb–N	Ta–N	Fe–N	Fe–C	V–O	Ta–O
$f^{(1)}$	2.694	2.952	4.078	3.463	3.214	2.720	2.566
$f^{(2)}$	−0.319	−0.375	0.245	−0.009	−0.350	−0.421	−0.399
$f^{(3)}$	0.506	0.520	0.507	0.689	0.759	0.518	0.717

TABLE X(a) Displacements evaluated by lattice model from experimentally measured dipole tensor and compound data.

Coordinates of neighbour atoms	V–N			Nb–N			Ta–N			Fe–N		
	U_x	U_y	U_z	U_x	U_y	U_z	U_x	U_y	U_z	U_x	U_y	U_z
(0 0 1)	0.0	0.0	0.531	0.0	0.0	0.448	0.0	0.0	0.471	0.0	0.0	0.444
(1 1 0)	−0.050	−0.050	0.0	−0.101	−0.101	0.0	−0.057	−0.057	0.0	−0.035	−0.035	0.0
(0 2 1)	0.0	0.092	0.065	0.0	0.046	0.034	0.0	0.029	0.031	0.0	0.0677	0.0478
(1 1 2)	0.011	0.011	0.045	0.021	0.021	0.070	0.029	0.029	0.063	0.0147	0.0147	0.0338
(0 0 3)	0.0	0.0	0.055	0.0	0.0	0.141	0.0	0.0	0.046	0.0	0.0	0.0294
(2 2 1)	0.023	0.0023	0.0065	−0.023	−0.023	−0.021	−0.017	−0.017	−0.012	−0.0065	−0.0065	0.0013
(1 3 0)	0.0	0.011	0.0	−0.0013	−0.026	0.0	0.0028	−0.0091	0.0	−0.0019	−0.0038	0.0
(0 2 3)	0.0	0.0089	0.0023	0.0	0.011	0.043	0.0	0.017	0.033	0.0	0.0093	0.0174
(1 3 2)	0.029	0.010	0.011	0.0056	0.0066	0.0064	−0.0013	0.0090	0.0050	0.0045	0.0056	0.0101
(2 2 3)	0.0023	0.0023	0.0099	−0.0023	−0.0023	0.0064	0.012	0.012	0.014	0.0056	0.0056	0.0114
(3 3 0)	−0.0011	−0.0011	0.0	−0.0074	−0.0074	0.0	−0.0088	−0.0088	0.0	−0.0044	−0.0044	0.0
(3 3 2)	0.0021	0.0021	0.0033	−0.0038	−0.0038	−0.0054	−0.0017	−0.0017	−0.0069	−0.0002	−0.0002	0.0017

Coordinates of neighbour atoms	V–O			Nb–O*			Ta–O			Fe–C		
	U_x	U_y	U_z	U_x	U_y	U_z	U_x	U_y	U_z	U_x	U_y	U_z
(0 0 1)	0.0	0.0	0.537	0.0	0.0	0.403	0.0	0.0	0.320	0.0	0.0	0.422
(1 1 0)	−0.064	−0.064	0.0	−0.106	−0.106	0.0	−0.079	−0.079	0.0	−0.064	−0.064	0.0
(0 2 1)	0.0	0.092	0.066	0.0	0.066	0.040	0.0	0.055	0.037	0.0	0.075	0.052
(1 1 2)	0.010	0.010	0.046	0.021	0.021	0.060	0.022	0.022	0.042	0.014	0.014	0.034
(0 0 3)	0.0	0.0	0.056	0.0	0.0	0.124	0.0	0.0	0.032	0.0	0.0	0.030
(2 2 1)	0.0010	0.0010	0.0063	−0.025	−0.025	−0.021	−0.019	−0.019	−0.012	−0.0093	−0.0093	−0.0005
(1 3 0)	−0.0006	0.0089	0.0	−0.0011	−0.022	0.0	0.021	−0.0022	0.0	−0.0025	−0.0045	0.0
(0 2 3)	0.0	0.0088	0.024	0.0	0.011	0.040	0.0	0.013	0.022	0.0	0.0092	0.0176
(1 3 2)	0.0029	0.0098	0.011	0.0069	0.010	0.0090	0.0030	0.011	0.0072	0.0047	0.0056	0.0103
(2 2 3)	0.0021	0.0021	0.010	−0.0028	−0.0028	0.0061	0.0088	0.0088	0.0098	0.0053	0.0053	0.0113
(3 3 0)	0.0005	0.0005	0.0	−0.0093	−0.0093	0.0	−0.0097	−0.0097	0.0	−0.0057	−0.0057	0.0
(3 3 2)	0.0019	0.0019	0.0034	−0.0041	−0.0041	−0.0057	0.0088	0.0088	0.0098	−0.0009	−0.0009	0.0012

*Compound data is estimated from $R_1 = 1.2$

TABLE X(b) Displacements evaluated by anisotropic elastic theory from experimentally measured dipole tensor

Coordinates of neighbour atoms	V–N			Nb–N			Ta–N			Fe–N		
	U_x	U_y	U_z	U_x	U_y	U_z	U_x	U_y	U_z	U_x	U_y	U_z
(0 0 1)	0.0	0.0	1.0380	0.0	0.0	1.5328	0.0	0.0	0.5837	0.0	0.0	0.3509
(1 1 0)	−0.0576	−0.0576	0.0	−0.0718	−0.0718	0.0	−0.0678	−0.0678	0.0	−0.0322	−0.0322	0.0
(0 2 1)	0.0	0.0038	0.0128	0.0	0.0059	0.0077	0.0	−0.0107	0.0182	0.0	−0.0120	0.0269
(1 1 2)	0.0222	0.0222	0.0700	0.0181	0.0181	0.0647	0.0361	0.0361	0.0883	0.0423	0.0423	0.0898
(0 0 3)	0.0	0.0	0.1153	0.0	0.0	0.1703	0.0	0.0	0.0649	0.0	0.0	0.0390
(2 2 1)	−0.0058	−0.0058	0.0035	−0.0080	−0.0080	0.0026	−0.0059	−0.0059	0.0019	0.0019	0.0019	0.0047
(1 3 0)	−0.0048	−0.0166	0.0	−0.0063	−0.0252	0.0	−0.0078	−0.0175	0.0	−0.0081	−0.0148	0.0
(0 2 3)	0.0	0.0167	0.0353	0.0	0.0178	0.0342	0.0	0.0205	0.0408	0.0	0.0222	0.0397
(1 3 2)	0.0010	0.0040	0.0079	0.0006	0.0032	0.0060	0.0022	0.0030	0.0111	0.0047	0.0044	0.0153
(2 2 3)	0.0060	0.0060	0.0165	0.0041	0.0041	0.0141	0.0123	0.0123	0.0248	0.0170	0.0170	0.0304
(3 3 0)	−0.0064	−0.0064	0.0	−0.0080	−0.0080	0.0	−0.0075	−0.0075	0.0	−0.0036	−0.0036	0.0
(3 3 2)	−0.0009	−0.0009	0.0027	−0.0018	−0.0018	0.0021	0.0001	0.0001	0.0029	0.0036	0.0036	0.0051

Coordinates of neighbour atoms	V–O			Nb–O			Ta–O			Fe–C		
	U_x	U_y	U_z	U_x	U_y	U_z	U_x	U_y	U_z	U_x	U_y	U_z
(0 0 1)	0.0	0.0	1.0858	0.0	0.0	1.3855	0.0	0.0	0.3955	0.0	0.0	0.3668
(1 1 0)	−0.0663	−0.0663	0.0	−0.0543	−0.0543	0.0	−0.0306	−0.0306	0.0	−0.0448	−0.0448	0.0
(0 2 1)	0.0	0.0012	0.0124	0.0	0.0106	0.0090	0.0	−0.0024	0.0148	0.0	−0.0147	0.0262
(1 1 2)	0.0228	0.0228	0.0727	0.0169	0.0169	0.0590	0.0264	0.0264	0.0624	0.0420	0.0420	0.0911
(0 0 3)	0.0	0.0	0.1206	0.0	0.0	0.1539	0.0	0.0	0.0439	0.0	0.0	0.0408
(2 2 1)	−0.0071	−0.0071	0.0033	−0.0057	−0.0057	0.0028	−0.0006	−0.0006	0.0030	−0.0008	−0.0008	0.0034
(1 3 0)	−0.0056	−0.0194	0.0	−0.0044	−0.0181	0.0	−0.0043	−0.0096	0.0	−0.0090	−0.0161	0.0
(0 2 3)	0.0	0.0172	0.0367	0.0	0.0164	0.0313	0.0	0.0150	0.0287	0.0	0.0221	0.0403
(1 3 2)	0.0008	0.0035	0.0080	0.0008	0.0041	0.0059	0.0023	0.0040	0.0088	0.0043	0.0032	0.0148
(2 2 3)	0.0061	0.0061	0.0171	0.0040	0.0040	0.0130	0.0093	0.0093	0.0180	0.0166	0.0166	0.0303
(3 3 0)	−0.0074	−0.0074	0.0	−0.0060	−0.0060	0.0	−0.0034	−0.0034	0.0	−0.0050	−0.0050	0.0
(3 3 2)	−0.0013	−0.0013	0.0027	−0.0011	−0.0011	0.0021	0.0014	0.0014	0.0029	0.0026	0.0026	0.0045

TABLE X(c) Displacements evaluated by isotropic elastic theory from experimentally measured dipole tensor

Coordinates of neighbour atoms	V–N			Nb–N			Ta–N			Fe–N		
	U_x	U_y	U_z	U_x	U_y	U_z	U_x	U_y	U_z	U_x	U_y	U_z
(0 0 1)	0.0	0.0	0.8075	0.0	0.0	0.8417	0.0	0.0	0.9465	0.0	0.0	0.9406
(1 1 0)	−0.0561	−0.0561	0.0	−0.0700	−0.0700	0.0	−0.0779	−0.0779	0.0	−0.0625	−0.0625	0.0
(0 2 1)	0.0	0.0007	0.0138	0.0	−0.0028	0.0099	0.0	−0.0052	0.0160	0.0	−0.0007	0.0222
(1 1 2)	0.0262	0.0262	0.0729	0.0279	0.0279	0.0731	0.0285	0.0285	0.0853	0.0272	0.0272	0.0887
(0 0 3)	0.0	0.0	0.0897	0.0	0.0	0.0935	0.0	0.0	0.1052	0.0	0.0	0.1045
(2 2 1)	−0.0050	−0.0050	0.0031	−0.0072	−0.0072	0.0011	−0.0084	−0.0084	0.0035	−0.0060	−0.0060	0.0064
(1 3 0)	−0.0050	−0.0151	0.0	−0.0063	−0.0188	0.0	−0.0070	−0.0209	0.0	−0.0056	−0.0168	0.0
(0 2 3)	0.0	0.0173	0.0356	0.0	0.0185	0.0359	0.0	0.0189	0.0417	0.0	0.0180	0.0432
(1 3 2)	0.0014	0.0042	0.0086	0.0012	0.0036	0.0072	0.0010	0.0031	0.0100	0.0013	0.0040	0.123
(2 2 3)	0.0078	0.0078	0.0181	0.0081	0.0081	0.0176	0.0082	0.0082	0.0212	0.0080	0.0080	0.0228
(3 3 0)	−0.0062	−0.0062	0.0	−0.0078	−0.0078	0.0	−0.0087	−0.0087	0.0	−0.0069	−0.0069	0.0
(3 3 2)	−0.0003	−0.0003	0.0027	−0.0009	−0.0009	0.0018	−0.0013	−0.0013	0.0031	−0.0006	−0.0006	0.0045

Coordinates of neighbour atoms	V–O			Nb–O			Ta–O			Fe–C		
	U_x	U_y	U_z	U_x	U_y	U_z	U_x	U_y	U_z	U_x	U_y	U_z
(0 0 1)	0.0	0.0	0.8458	0.0	0.0	0.7561	0.0	0.0	0.6510	0.0	0.0	0.9652
(1 1 0)	−0.0650	−0.0650	0.0	−0.0512	−0.0512	0.0	−0.0396	−0.0396	0.0	−0.0732	−0.0732	0.0
(0 2 1)	0.0	−0.0019	0.0134	0.0	0.0023	0.0110	0.0	0.0023	0.0133	0.0	−0.0046	0.0214
(1 1 2)	0.0269	0.0269	0.0756	0.0260	0.0260	0.0670	0.0208	0.0208	0.0601	0.0271	0.0271	0.0902
(0 0 3)	0.0	0.0	0.0940	0.0	0.0	0.0840	0.0	0.0	0.0723	0.0	0.0	0.1072
(2 2 1)	−0.0065	−0.0065	0.0027	−0.0042	−0.0042	0.0020	−0.0032	−0.0032	0.0035	−0.0079	−0.0079	0.0059
(1 3 0)	−0.0058	−0.0175	0.0	−0.0046	−0.0138	0.0	−0.0036	−0.0106	0.0	−0.0066	−0.0196	0.0
(0 2 3)	0.0	0.0178	0.0370	0.0	0.0172	0.0328	0.0	0.0137	0.0293	0.0	0.0180	0.0439
(1 3 2)	0.0012	0.0037	0.0086	0.0015	0.0046	0.0073	0.0013	0.0038	0.0077	0.0010	0.0030	0.0121
(2 2 3)	0.0079	0.0079	0.0187	0.0078	0.0078	0.0164	0.0063	0.0063	0.0152	0.0078	0.0078	0.0230
(3 3 0)	−0.0072	−0.0072	0.0	−0.0057	−0.0057	0.0	−0.0044	−0.0044	0.0	−0.0081	−0.0081	0.0
(3 3 2)	−0.0008	−0.0008	0.0026	0.0	0.0	0.0021	0.0001	0.0001	0.0027	−0.0012	−0.0012	0.0043

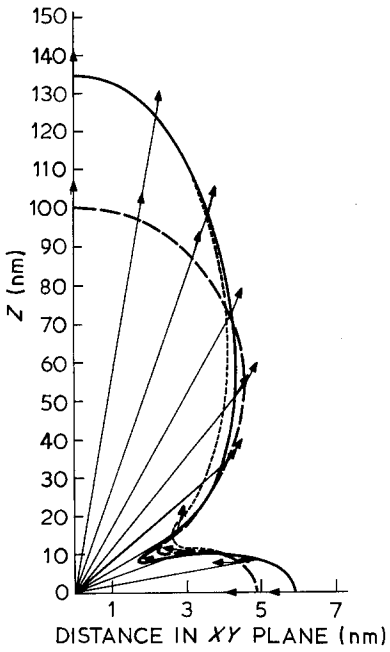

Figure 6 Locus of elastic displacements of constant magnitude for Nb–N system. Symbols as for Fig. 5. $u_0 = 0.843 \times 10^{-5}$ nm $\alpha = -0.24$.

Treating this as a constant has allowed us to develop a pseudo structure of the NaCl type even though this structure is not always observed. A correlation factor between this volume and the effective volume due to a filled octahedron in a dilute solution data has been found. Therefore, one can determine the atomic volume from a M_2I compound, then calculate the atomic volume of the MI compound, and then estimate d_2 and V_I^*. Alternatively, the required volume change in the dilute interstitial solution is obtained from the shape factor S and the second-neighbour strain ε_{11}. This correlation of parameters allows estimates to be made of the dipole tensor in two ways.

The core region is conveniently defined as the six neighbours of an interstitial which tend to be at nearly equal distances in the form of a regular octahedron. The second-neighbour distance about an interstitial undergoes only a small negative displacement and can be estimated from known crystallographic data.

Plots of the elastic displacement field, obtained from anisotropic elasticity theory show that there is a major positive disturbance along the tetragonal axis and a minor disturbance in the perpendicular directions. When the anisotropy factor is large and positive, the disturbance along the C axis is reduced (Fe–C) while when it becomes negative (Nb–N) it is expanded relative to the isotropic calculation. For anisotropic materials, differences are found for atoms located in (0 0 1) and (0 1 1) planes. That is, the displacement field is not symmetrical about the tetragonal axis but only within planes of fixed orientation.

Although, V–O fits the same overall pattern as the nitrides, Ta–O appears to be out of the expected error band. It is known that oxygen can show a tendency for ionic bonding and a higher degree of electron exchange with metal orbitals. Consequently, the estimates developed in this paper become questionable with interstitial systems containing oxygen and probably should be limited only to those containing nitrogen and carbon.

TABLE XI Anisotropic factor, α

V	Nb	Ta	Cr	Mo	W	Fe
−0.12	−0.24	0.31	−0.42	−0.44	0.01	0.68

Acknowledgements

The authors are grateful to Dr E. J. Savino for assistance in calculations involving the Green function. Funding for this research came from Office of Naval Research Grant No N00014-83-K-750, P00004.

References

1. G. LEIBFRID and N. BREUER, "Point Defects in Metals I", Springer Tracts in Modern Physics, Vol. 81 (1978).
2. S. I. RAO and C. R. HOUSKA, *Nucl. Instrum. Meth.* **B18** (1986) 47.
3. *Idem., ibid.* **B27** (1987) 396.
4. V. K. TEWARY, *J. Phys. F.* **3** (1973) 1515.
5. E. S. FISHER, D. G. WESTLAKE and S. T. OCKERS, *Phys. Status Solidi a* **28** (1975) 591.
6. H. PEISL, in "Hydrogen in Metals" (edited by G. Alefeld and J. Wolkl), Vol. 1. (Springer, Berlin, 1979).
7. S. A. BRADFORD and O. N. CARLSON, *Trans. Amer. Soc. Met.* **55** (1962) 169.
8. H. PFEIFFER and H. PEISL, *Phys. Lett.* **A60** (1977) 363.
9. A. MAGERL, B. BERRE and G. ALEFEDE, *Phys. Status Solidi a* **36** (1976) 161.
10. M. A. PICK and R. BAUSCH, *J. Phys. F* **6** (1976) 1751.
11. D. RICHTER and D. O. WELCH, *Scripta Metall.* **12** (1978) 831.
12. A. I. SHIRLEY, C. K. HALL and N. J. PRINCE, *Acta Metall.* **31** (1983) 985.
13. L. E. TOTH, in "Transition Metal Carbides and Nitrides", (Academic, New York, 1971) p. 40.
14. E. C. BAIN, *Trans AIME* **70** (1924) 25.
15. A. G. KHACHATURYAN and G. A. SHATALOV, *Acta Metall.* **23** (1975) 1089.
16. P. WILLARS and L. D. CALRERT, in "Pearson's Handbook of Crystallographic Data for Intermetallic Phases", (ASM, Metals Park, 1985).
17. H. J. GOLDSCHMIDT, in "Interstitial Alloys", (Plenum, New York, 1967).
18. H. W. KING, *J. Mater. Sci.* **1** (1966) 79.
19. A. K. VOLKOV *et al., Fiz. Metal. Metalloved,* **31** (1971) 103.
20. F. F. MILILLO and D. I. POTTER, *Met. Trans* **9A** (1978) 283.
21. R. SPEISER *et al., J. Met.* **4** (1952) 275.
22. J. L. HENRY, *et al., J. Less-Common Metals* **21** (1970) 115.
23. *Idem., ibid.* **25** (1971) 39.
24. Z. NISHIYAMA, in "Martensitic Transformation", (Academic, New York, 1978) p. 19.
25. M. S. BLANTER and A. G. KHACHATURYAN, *Met. Trans.* **94** (1978) 753.
26. H. A. WRIEDT, N. A. GOKEEN and R. H. NAFZIGER, *Bull. Alloy Phase Diagram* **8** (1987) 355.
27. M. A. SHTREMEL *et al., Phys. Met. Metall.* **57** (1984) 168.
28. D. T. KEATING and A. N. GOLAND, *Acta Metall.* **15** (1967) 1805.
29. J. D. ESHELBY, *J. Appl. Phys.* **25** (1954) 255.
30. P. H. DEDERICHS, *J. Phys. F.* **3** (1973) 471.
31. S. RAO, E. J. SAVINO and C. R. HOUSKA, *Met. Res. Symp. Proc.,* Materials Research Society, Vol. 82 (1987).

Received 14 March
and accepted 17 August 1989